DMACM-Caged Adenosine Nucleotides: Ultrafast Phototriggers for ATP, ADP, and AMP Activated by Long-Wavelength Irradiation**

Daniel Geißler,[a] Wolfgang Kresse,[b] Burkhard Wiesner,[a] Jürgen Bendig,[c] Helmut Kettenmann,[b] and Volker Hagen*[a]

The development of new photocleavable adenosine nucleotides based on the photochemistry of [7-(dimethylamino)coumarin-4-yl]methyl (DMACM) esters is described. The phototriggers liberate adenosine triphosphate (ATP), diphosphate, and monophosphate upon UV/Vis irradiation between 334 and 405 nm. The efficiency of photocleavage at long wavelengths is high as a result of a combination of appropriate quantum yields and intensive absorptivities. By using time-resolved fluorescence spectroscopy, we determined a lower limit of $1.6 \times 10^9\ s^{-1}$ for the rate constant of the release of ATP from DMACM-caged ATP. The favorable properties of DMACM-caged ATP were confirmed in physiological studies by confocal laser scanning microscopy. We were able to uncage DMACM-caged ATP in cultures of mouse astrocytes and in brain tissue slices from mice and were also able to measure the effect of photoreleased ATP on the cellular response of astrocytes, namely the ability of the ATP to evoke Ca^{2+} ion waves.

KEYWORDS:

astrocytes · caged compounds · calcium · nucleotides · protecting groups

Introduction

Controlled temporal and spatial release of biomolecules from photolabile precursors, known as "caged" molecules, has become increasingly important in biological studies.[1] When caged, a biomolecule is rendered biologically inactive by derivatization with a photolabile protecting or caging group. The caged form does not evoke biological responses when applied. Flash photolysis with UV light cleaves the caging group and generates the biologically active molecule. In this way, fast jumps in the concentration of the biomolecule can be achieved at a defined location.

Caged adenosine 5′-triphosphates (caged ATPs) are frequently used caged biomolecules. The derivatives most commonly used for protection of ATP are P^3-(2-nitrobenzyl),[2] P^3-[1-(2-nitrophenyl)ethyl] (NPE),[2–4] or P^3-[1-(4,5-dimethoxy-2-nitrophenyl)ethyl] (DMNPE) esters[5]. However, the nitrophenylalkyl esters photolyze relatively slowly and display rather low photoefficiencies upon irradiation at $\lambda > 360$ nm.[6] The recently reported desoxybenzoinyl-caged (desyl-caged) ATPs[7–9] and *p*-hydroxyphenacyl-caged (pHP-caged) ATP[6, 10] seem to have more favorable properties, but their small extinction coefficients at longer wavelengths permit only small jumps in ATP concentration at $\lambda > 360$ nm, whilst short-wavelength light has poor tissue penetration because of absorption by intra- and extracellular chromophores in this region of the electromagnetic spectrum. Furthermore, the use of desyl-caged ATPs is limited by their sensitivity to solvolysis in aqueous buffer solutions.[6, 7] Caged adenosine 5′-diphosphates (ADPs) and adenosine 5′-monophosphates (AMPs) have been introduced as the nitrophenylalkyl derivatives.[3] As in the case of the nitrophenylalkyl-caged ATPs, these compounds have disadvantages that limit their applications.

We recently reported the use of [7-(dialkylamino)coumarin-4-yl]methyl esters of adenosine 3′,5′-cyclic monophosphate (cAMP) and guanosine 3′,5′-cyclic monophosphate (cGMP) as highly efficient, ultrafast phototriggers for cyclic nucleotides that can be activated by long-wavelength radiation.[11, 12] With the aim of developing better phototriggers for ATP, ADP, and AMP, we have also applied the concept to the adenosine nucleotides. Here we describe the synthesis and photochemical properties of

[a] *Dr. V. Hagen, Dipl.-Ing. D. Geißler, Dr. B. Wiesner*
Forschungsinstitut für Molekulare Pharmakologie (FMP)
Robert-Rössle-Strasse 10, 13125 Berlin (Germany)
Fax: (+49) 30-94793-159
E-mail: hagen@fmp-berlin.de

[b] *Dipl.-Phys. W. Kresse, Prof. Dr. H. Kettenmann*
Max-Delbrück-Centrum für Molekulare Medizin (MDC)
Robert-Rössle-Strasse 10, 13125 Berlin (Germany)

[c] *Prof. Dr. J. Bendig*
Institut für Chemie der Humboldt-Universität
Brook-Taylor-Strasse 2, 12489 Berlin (Germany)

[**] *DMACM = [7-(dimethylamino)coumarin-4-yl]methyl; ATP = adenosine 5′-triphosphate; ADP = adenosine 5′-diphosphate; AMP = adenosine 5′-monophosphate.*

Supporting information for this article is available on the WWW under http://www.chembiochem.org or from the author.

  1439-4227/03/04/2-3 $ 20.00+.50/0 ChemBioChem **2003**, 4, 162 – 170

[7-(dimethylamino)coumarin-4-yl]methyl (DMACM) esters of adenosine nucleotides as new phototriggers for ATP, ADP, and AMP. The novel DMACM caging group shows an intensive absorption maximum at around 400 nm and should, as in the case of caged cyclic nucleotides, allow efficient photorelease of the adenosine nucleotides at excitations between 330 and 440 nm.

We used cultured mouse astrocytes in combination with confocal laser scanning microscopy (CLSM) to test the DMACM-caged ATP **2** under physiological conditions. Astrocytes represent the largest cell population in the brain and are now recognized, in concert with the neurons, as important elements for signaling. Astrocytes are a subtype of glia and not only are they important for normal brain function, but they also change their properties in response to pathologic events related to, for example, Alzheimer's disease or stroke. It has recently become evident that glial cells express a large repertoire of neurotransmitter receptors, and that purinergic receptors in particular represent a common receptor system for all the glial cell types. Purinergic receptors are an important prerequisite for the generation of astrocytic Ca^{2+} ion waves, a specific form of glial communication observed both in vitro and in situ.[13] Astrocytes express both ionotropic (P2X) and metabotropic ATP receptors (P2Y), the latter of which are more abundant.[14] Binding of ATP to P2Y receptors gives rise to an increase in intracellular inositol 1,4,5-tris(phosphate) (IP_3); this results in IP_3-driven mobilization of Ca^{2+} ions from internal Ca^{2+} stores.[15] These increases in cytoplasmic Ca^{2+} ion concentration ($[Ca^{2+}]_i$) in response to ATP can be recorded with fluorescent Ca^{2+}-sensitive dyes such as fluo-3.

To test the release of **2** in a tissue and to measure its impact on cells, we used acutely isolated brain slices in which we preferentially labeled astrocytes with a Ca^{2+} indicator. We were able to uncage **2** in brain tissue slices and to measure the effect of photogenerated ATP on the cellular response of the astrocytes, that is, the ability of **2** to evoke Ca^{2+} ion waves.

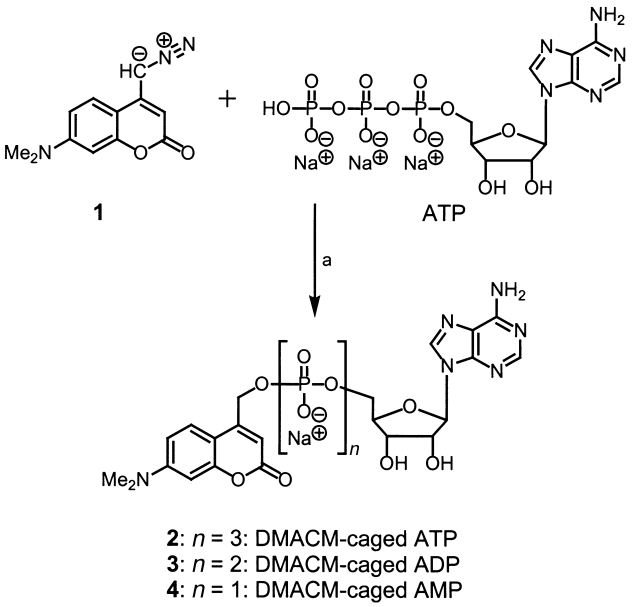

Scheme 1. *Synthesis of **2** – **4** (Method A): a) $CHCl_3/H_2O$ (1:1, v/v), RT, 24 h, pH 4.2.*

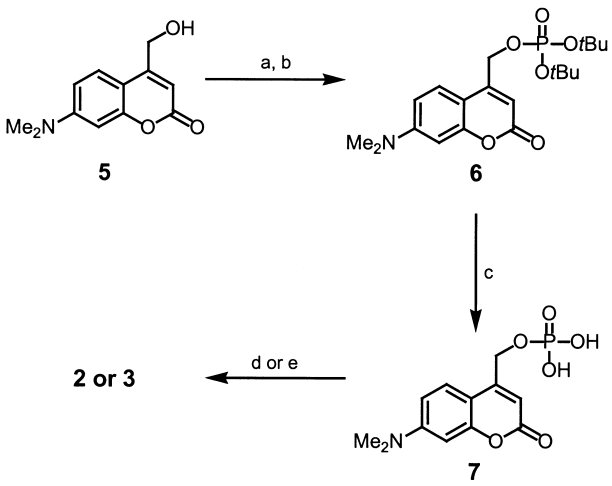

Scheme 2. *Synthesis of **2** and **3** (Method B): a) $Et_2NP(OtBu)_2$, 1H-tetrazole, THF, −20 °C → RT, 12 h; b) tBuOOH, Et_3N, THF, 0 °C → RT, 4 h; c) TFA, CH_2Cl_2, 0 °C, 6 h; d) ADP, Im_2CO, HMPA, RT, 3 d; e) AMP, Im_2CO, DMF, RT, 3 d. Im_2CO = carbonyldiimidazole, HMPA = hexamethylphosphoric triamide, DMF = dimethylformamide.*

Results and Discussion

Synthesis

The synthesis of the DMACM-caged adenosine nucleotides **2** – **4** followed two different strategies. The first synthetic route (Method A) involved alkylation of ATP with 4-(diazomethyl)-7-(dimethylamino)coumarin (**1**; Scheme 1).[16a] In the second approach (Method B, Scheme 2), the DMACM phosphate **7** was prepared in 46% overall yield from the alcohol **5**[12] by treatment with a phosphoramidite, oxidation with *tert*-butyl (*t*Bu) hydroperoxide to the ester **6**, and subsequent hydrolysis of the *tert*-butoxy groups with trifluoroacetic acid (TFA). Compound **7** was coupled with carbonyldiimidazole-activated ADP or AMP by the general procedure described for the NPE or pHP esters of ATP[2, 4, 6] or the [7-(diethylamino)coumarin-4-yl]methyl ester of cytidine diphosphate.[17] Method A gave DMACM-caged ATP (**2**) in only 1.7% yield. This low yield is attributed to the relatively low reactivity of 4-(diazomethyl)coumarins.[18] Because ADP and AMP are formed from ATP under the reaction conditions, DMACM-caged ADP (**3**) and DMACM-caged AMP (**4**) were also isolated in 3.5% and 1.7% yields, respectively. The mixture was separated by preparative reversed-phase HPLC. Method B afforded **2** and **3** in nonoptimized 20% and 23% yields, respectively. Clearly, Method B is superior to Method A for the synthesis of **2** and **3**. Contamination of **2** – **4** with free nucleotides was less than 0.5% as judged by analytical HPLC.

The hydrolytic stability of a caged compound in physiological salt solutions is important for its use as a phototrigger. HPLC analysis showed that **2** – **4** are stable in aqueous media. Solutions of the caged compounds in *N*-2-hydroxyethylpiperazine-*N*′-2-ethanesulfonic acid (HEPES) buffer at pH 7.2 showed losses of less than 0.5% over a 24-h period.

Photochemical properties

The absorption spectra of **2** – **4** are characterized by the intensive $S_0 - S_1$ absorption maxima at around 385 nm (Table 1, Figure 1), which allow efficient activation of the caged compounds between 330 – 440 nm. This is desirable for cell biological applications because it is possible to reduce the light energy in the uncaging reaction to minimize cell damage and chromophore bleaching.

Table 1. *Long-wavelength absorption maximum λ_{abs}^{max}, extinction coefficient ε^{max}, photochemical quantum yield Φ_{chem}, fluorescence maximum λ_f^{max}, fluorescence quantum yield Φ_f, and fluorescence lifetime τ_f of* ***2*** *–* ***4****,* ***5****, and the axial diastereomer of DMACM-caged cAMP.*

Compound	λ_{abs}^{max} [nm]	ε^{max} [M^{-1} cm^{-1}]	Φ_{chem}[c]	λ_f^{max} [nm]	Φ_f[d]	τ_f [ns]
2[a]	385	15300	0.086	496	0.217	1.71
3[a]	385	15000	0.063	496	0.253	1.98
4[a]	385	14300	0.072	496	0.235	1.88
5[b]	378	17800	-	491	0.214	1.70
DMACM-cAMP[b]	394	17200	0.28	482	0.008	$\ll 0.2$

[a] HEPES, pH 7.2. [b] MeOH/HEPES 1:4 (v/v), pH 7.2. [c] Error limit $\pm$ 0.01. [d] Error limit $\pm$ 0.002.

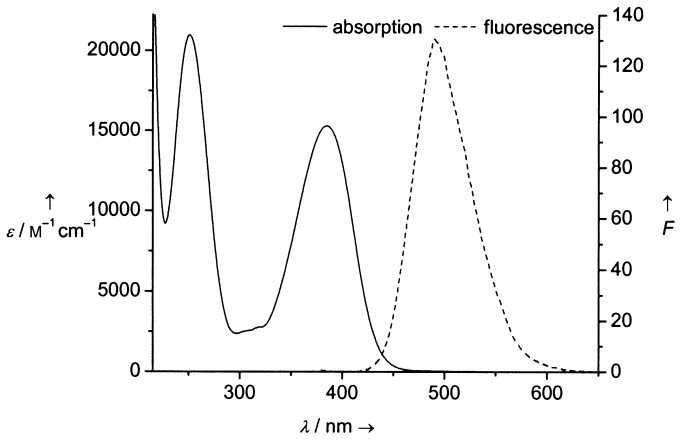

Figure 1. *UV/Vis absorption and fluorescence spectra of a 25 μM solution of* ***2*** *in HEPES buffer, pH 7.2.*

Irradiation of **2** – **4** at 330 – 440 nm in aqueous buffer solutions resulted in the photorelease of ATP, ADP, or AMP, together with **5** (Scheme 3). HPLC measurements confirmed the clean photogeneration of the nucleotides and **5** from **2** – **4**. As regards the mechanism of the underlying photochemical conversion, we assume it to be a photochemical S_N1 reaction (solvent-assisted photoheterolysis) analogous to that of (7-methoxycoumarin-4-yl)methyl-caged cAMP.[19] No trace of radical-derived products was observed for any of the compounds **2** – **4**. The quantum yields (Φ_{chem}) for the disappearance of caged nucleotides were 0.06 – 0.09 (Table 1), determined by the relative method by use of a standard in combination with analytical HPLC. These values are significantly lower than the quantum yield of DMACM-caged

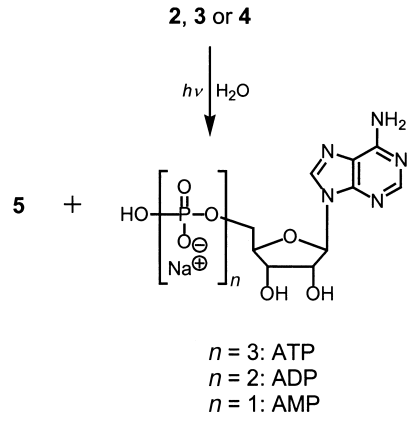

Scheme 3. *Photolysis of* ***2*** *–* ***4*** *in HEPES buffer solutions, pH 7.2.*

cAMP[11, 12] (Table 1), a result showing that the cAMP anion is a better leaving group than the ATP, ADP, or AMP anion.

The fluorescence quantum yields (Φ_f) of **2** – **4** are relatively high and comparable to that of **5** (Table 1). Therefore, in contrast to the case of DMACM-caged cAMP, no enhancement of the fluorescence should be expected upon photolysis of **2** – **4**. The fluorescence lifetimes (τ_f) are 1.71 – 1.98 ns for **2** – **4** and 1.70 ns for **5** (Table 1). In order to measure the magnitude of the rate constant of product formation during photolysis of **2**, time-resolved fluorescence spectroscopy was used. The fluorescence decay curve of the alcohol **5** is strictly mono-exponential (Figure 2). Analysis of the fluorescence decay of **2** at low-intensity excitation (Figure 3; nitrogen laser, $\lambda_{exc} = 337$ nm, pulse half-width about 0.5 ns) also shows a mono-exponential decay, and this decay is described by the fluorescence lifetime

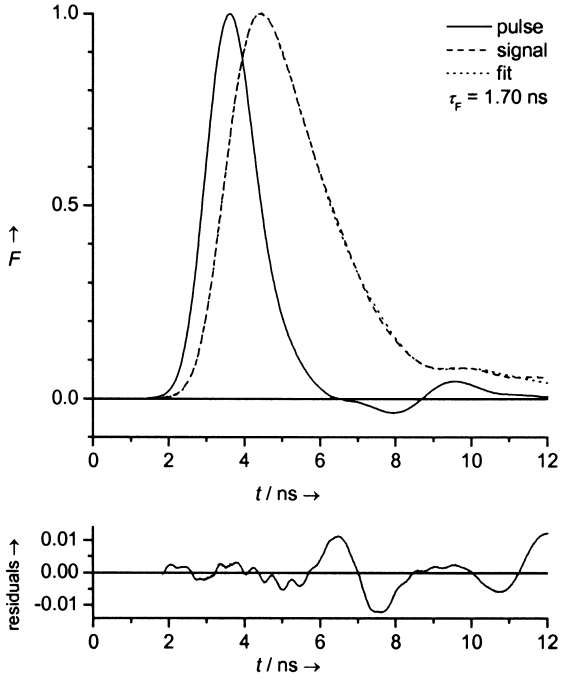

Figure 2. *Fluorescence decay curve of a 25 μM solution of* ***5*** *in methanol/HEPES buffer (1:4, v/v), pH 7.2; $\lambda_{exc} = 337$ nm, $\lambda_{em} = 500$ nm.* F = *relative fluorescence intensity.*

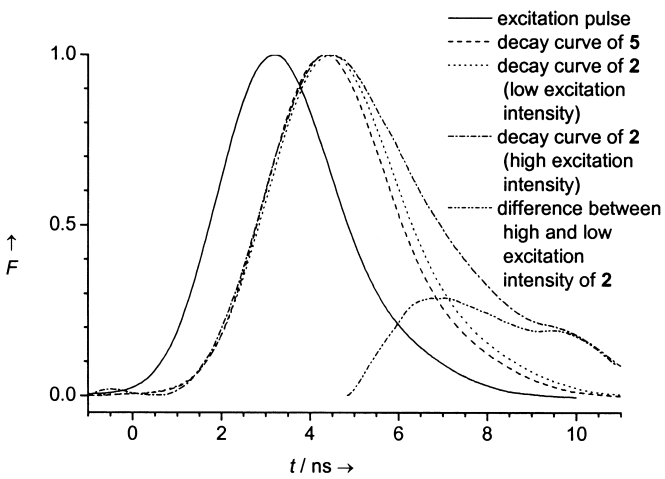

Figure 3. *Fluorescence decay curves of a 30 μM solution of **2** and **5** in methanol/HEPES buffer (1:4, v/v), pH 7.2, $\lambda_{exc} = 337$ nm, $\lambda_{em} = 500$ nm. F = relative fluorescence intensity.*

$\tau_f = 1.71$ ns. At high-intensity one-pulse excitation of **2** (Figure 3), more complex decay behavior is observed. Within the timescale of the fluorescence rise (0 – 4 ns) the decay curves with low- and high-intensity excitation are very similar. At timescales longer than 4 ns, however, the high-intensity decay is much slower than the low-intensity decay. This difference occurs because the high-intensity decay curve is shaped by the mono-exponential decay of **2** and *additionally* by the decay of the alcohol **5** formed within the pulse duration. The high-intensity decay curve is therefore the superimposition of these two signals (Figure 3). Mathematical deconvolution[20] of the experimentally determined high-intensity decay curve gives a rate constant of alcohol and ATP formation larger than $1.6 \times 10^9\ s^{-1}$ (i.e., the subnanosecond time scale is achieved for the liberation of ATP). The measured rate constant is comparable to those of the coumarinylmethyl-caged cAMPs[11, 12, 19] and means that the rate of ester cleavage is at least six to seven orders of magnitude faster than those reported for the cleavage of the *o*-nitrobenzyl esters of ATP[3, 5, 21] and three orders of magnitude faster than that of pHP-caged ATP.[6, 10] The high rate of photorelease corroborates the proposed photolytic reaction mechanism.

Table 2 gives the efficiencies of photorelease of **2** in comparison to those of the NPE- and DMNPE-caged ATPs in HEPES buffer solutions at different wavelengths. The results show that **2** was converted twice as efficiently as the nitrophenylethyl-caged ATPs under identical experimental conditions at 365 nm, and ten times more efficiently at 405 nm.

Table 2. *Comparison of the efficiency (in %) of the photorelease of ATP from 25 μM solutions of NPE-caged ATP, DMNPE-caged ATP, and **2** in HEPES buffer (pH 7.2) at different wavelengths.*

Phototrigger	$\lambda_{exc} = 334$ nm			$\lambda_{exc} = 365$ nm			$\lambda_{exc} = 405$ nm		
	E [mJ]			*E* [mJ]			*E* [mJ]		
	90	900	9000	90	900	9000	90	900	9000
NPE-caged ATP	7	55	> 99	3	22	93	< 1	2	12
DMNPE-caged ATP	4	35	> 99	3	28	96	< 1	4	30
2	3	24	92	7	46	> 99	6	41	> 99

Physiological experiments

The biological activity of our caged construct was tested in cell cultures and in tissue slices. ATP is known to elicit transient $[Ca^{2+}]_i$ increases in astrocytes. To measure the response of uncaged ATP, cytosolic Ca^{2+} concentrations were recorded from confluent astroglial cultures stained with the Ca^{2+} indicator fluo-3 (Figure 4a, upper left panel). UV irradiation alone did not evoke any change in fluo-3 fluorescence when it is taken into account that some cells exhibited spontaneous Ca^{2+} oscillations, which sometimes coincided with the UV irradiation. When 500 μM of caged ATP was applied it did not trigger a Ca^{2+} response; this observation indicates that **2** is indeed biologically inactive and reasonably stable against hydrolysis (data not shown). A period of 60 s after the application of **2**, UV light ($\lambda = 364$ nm) from an argon ion laser was used to illuminate a confined area (diameter 10 – 40 μm) within the scanning area of the culture for 250 ms. An average 1.8 ± 0.5 s after UV irradiation, an increase in fluorescence was recorded in cells close to the UV spot. Over the next 30 s, fluorescence also increased in cells surrounding the irradiated spot, which resulted in a fluorescence wave propagating from the original point of stimulation in a circular fashion, with the maximal extension depending on the size of the illumination area and the applied concentration of **2** (Figure 4a).

When we focused the UV beam on a small cell-free area within the astrocytic monolayer (Figure 4b and c), the spreading Ca^{2+} signal in the surrounding cells was similar to that seen in experiments in which liberation of ATP occurred in cell-containing areas (data not shown). This result further indicates that the spreading fluorescence signal was triggered by uncaged ATP, rather then cell damage. We successfully elicited astrocytic Ca^{2+} responses up to three times, provided that the cells were allowed to recover for at least 20 s (Figure 4c). In addition, the amplitude of the response is negatively correlated with increasing distance from the release area. The Ca^{2+} response was transient and showed the typical time course of an ATP-triggered signal: a fast increase in cytosolic Ca^{2+} ion concentration and a subsequent slow decay back to the concentration level prior to the ATP-triggered response.[13]

To investigate correlation between the propagating Ca^{2+} signal and the diffusion of photoliberated ATP from its release area, we analyzed the relationship between distance and onset times of the Ca^{2+} responses. One typical experiment is shown in Figure 4d. The best nonlinear least-squares fit of Equation (3) to the experimental data assumes a threshold concentration of liberated ATP of 0.44 ± 0.14 μM (mean ± standard error of mean (SEM); $R^2 = 0.66 \pm 0.16$; see the Experimental Section for details). The mean delay between UV irradiation and the first Ca^{2+} response was 0.8 ± 0.4 s ($n = 5$) in vitro. The obtained threshold concentration is in the order of the EC_{50} value (the concentration that gives half the maximum effect; 4.3 μM) reported for P2Y-receptor-triggered Ca^{2+} responses in acutely isolated astrocytes.[22]

To test whether ATP can be uncaged from **2** in tissue, we prepared frontal brain slices from five-day-old mice. We restricted our analysis to the corpus callosum, since all somata

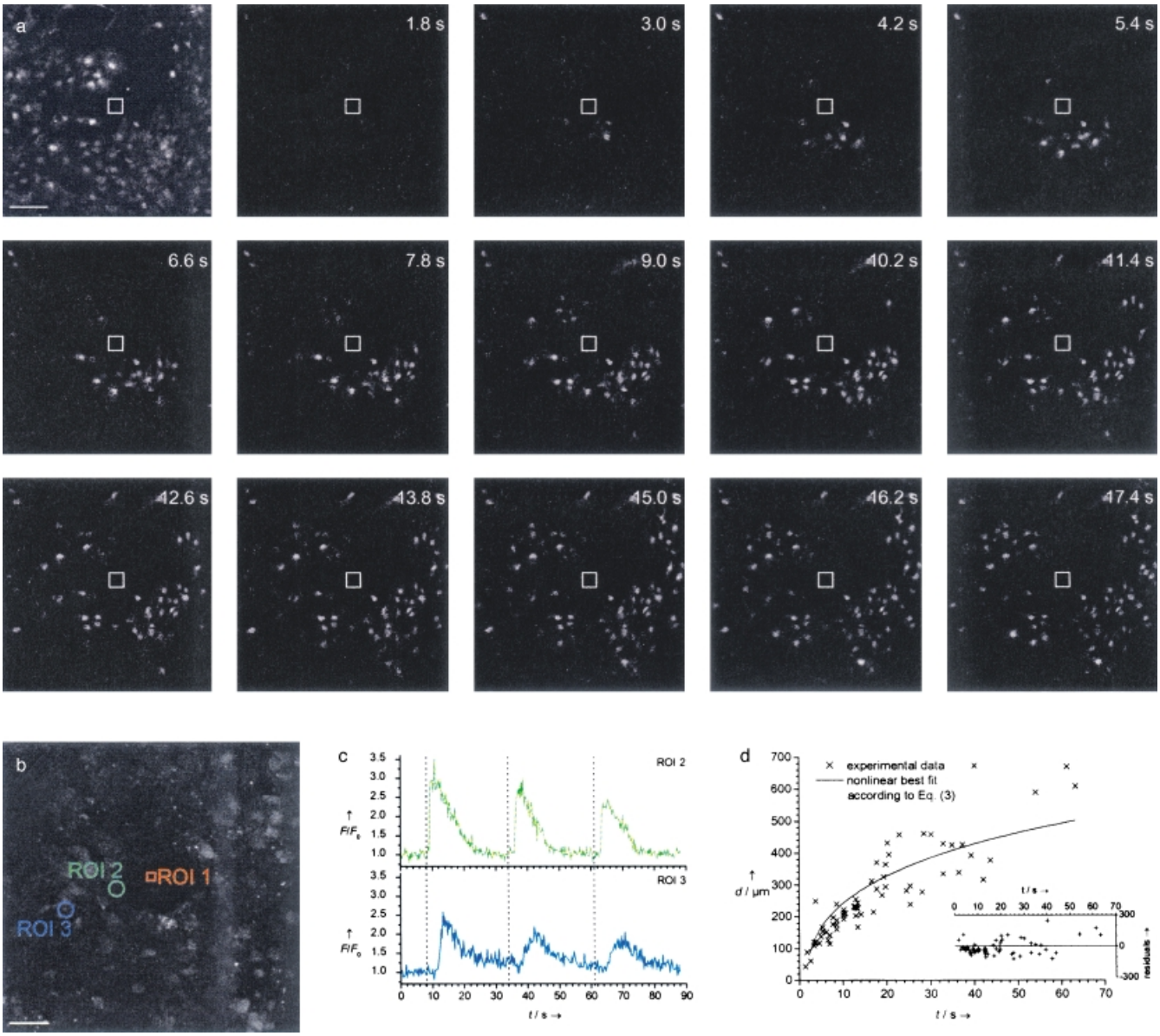

Figure 4. *Focal photorelease of ATP in cultured mouse astrocytes. a) Time series of differential pictures taken sequentially after the photolytic liberation of ATP from its caged precursor* ***2****. The top left picture shows the resting fluorescence of the cultured astrocytic monolayer prior to UV irradiation. Each subsequent picture shown is presented as a pixel-by-pixel difference picture of the picture recorded at the time point indicated minus the top left picture. Times indicated are given relative to the end of the photolytic exposure (254 ms). Approximately 2.6 s after the end of the UV irradiation, cells in close proximity to the illumination area (square, 39.6 × 39.6 μm) start to show an increase in intracellular Ca^{2+} ion concentration, as seen by the increased fluo-3 fluorescence. With increasing distance from the release area, the rise in $[Ca^{2+}]_i$ is increasingly delayed. The scan area is 575.8 × 575.8 μm. The sequence was recorded with a sampling rate of 2.5 Hz. White scale bar in the top left picture = 100 μm. b) Regions of interest (ROIs) 2 and 3, which represent individual astrocytes at different spatial distance from the focal illumination area (ROI 1, square), were used to analyze the distance/time relationship of the onset of the transient Ca^{2+} response as shown in (c). The scan area is 394.9 × 382.2 μm, the sampling frequency 4 Hz, and the white scale bar (lower left) = 50 μm. c) Kinetics of the Ca^{2+} ion transients of ROIs 2 and 3 shown in (b). Traces represent the mean fluorescence in each ROI relative to the fluorescence before UV irradiation. Compound* ***2*** *was irradiated three times (3 × 307 ms, dashed lines) resulting in three Ca^{2+} responses. d) Analysis of the relationship between the propagating Ca^{2+} signal and the diffusion of ATP in culture. Data points show the onset time of the Ca^{2+} response with respect to the respective distance to the illumination area. The curve shows the best fit of Equation (3) to the datapoints with the free parameters $c_{crit} = 0.17 \pm 0.04$ μM and $t_{delay} = 1.7 \pm 0.3$ s ($R^2 = 0.73$).*

in this white matter tract are from glial cells (Figure 5a). The cells were loaded with fluo-3 by a procedure described previously[23] to allow for the detection of changes in $[Ca^{2+}]_i$. As in the culture, addition of 1 mM **2** to the slice did not result in a fluorescence signal. Excitation of an area approximately 20 μm in diameter triggered a fluorescence signal. As in the culture, the Ca^{2+} signal spread in an approximately circular fashion from the point of stimulation, with a limited extension of about 250 ± 50 μm. Again, the kinetics of the Ca^{2+} transient in individual cells showed the typical time course, as described previously (Figure 5b).[13]

We analyzed the relationship between distance and onset times of the Ca^{2+} responses in a similar way to that described for the data obtained in the culture (Figure 5c). Here, nonlinear

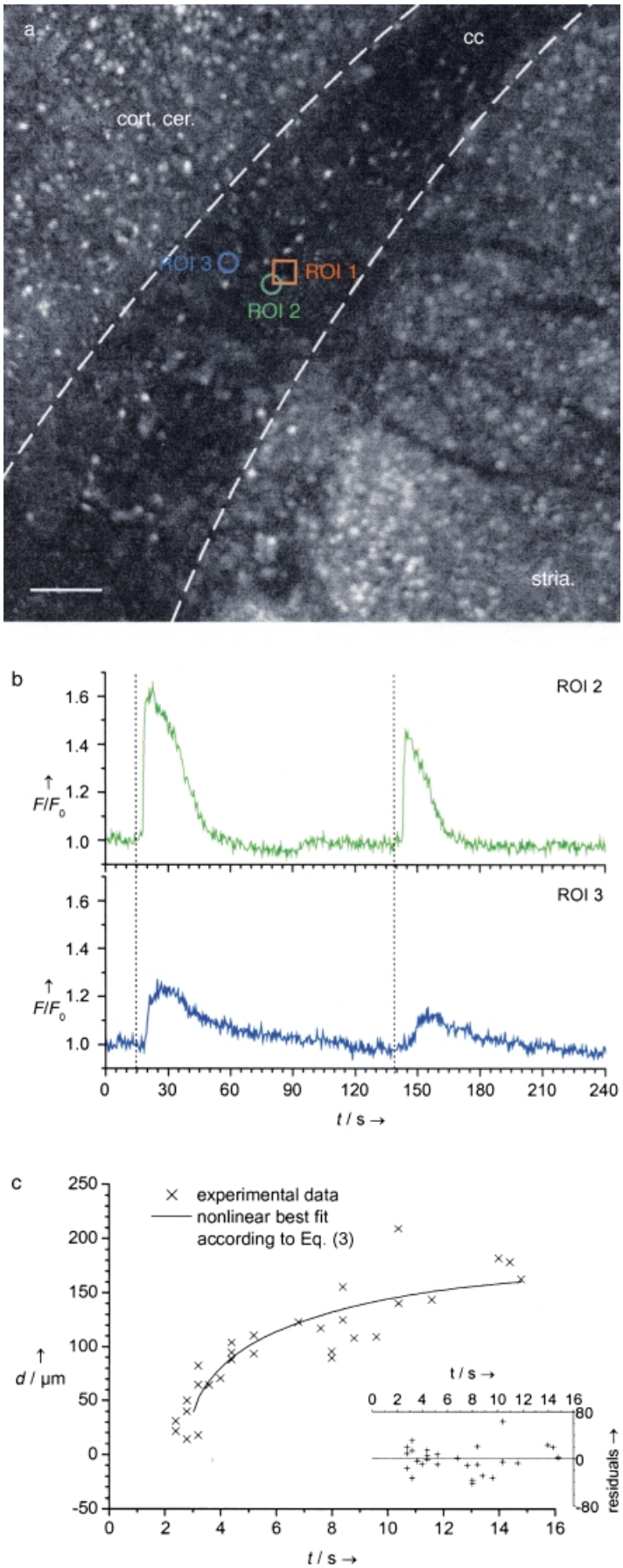

least-squares fitting of Equation (3) resulted in a threshold concentration for the propagating Ca^{2+} wave of 4.4 ± 0.8 µM (mean ± SEM; $R^2 = 0.54 \pm 0.14$). The mean delay between UV irradiation and the first Ca^{2+} response in situ was 3.1 ± 0.3 s ($n = 3$).

Conclusions

Ultrafast photorelease of the adenosine nucleotides ATP, ADP, and AMP can be achieved at wavelengths greater than 360 nm in amounts sufficient to trigger biological responses from single cells both in cell cultures and in tissue slices. This approach shows great potential for the study of time- and spatially resolved aspects of ATP-, ADP-, and AMP-dependent cellular processes under nondamaging light conditions.

Experimental Section

Materials: 4-(Diazomethyl)-7-(dimethylamino)coumarin (**1**) was prepared by SeO_2 oxidation of 7-(dimethylamino)-4-methylcoumarin to the corresponding coumarin-4-carbaldehyde, followed by a triethylamine-mediated Bamford – Stevens reaction of its tosylhydrazone according to a procedure described for 4-(diazomethyl)-7-(diethylamino)coumarin.[18] 7-(Dimethylamino)-4-(hydroxymethyl)coumarin (**5**) was synthesized as described previously.[12] The preparation of [7-(dimethylamino)coumarin-4-yl]methyl di-*tert*-butyl phosphate (**6**) and [7-(dimethylamino)coumarin-4-yl]methyl phosphate (**7**) is described in the Supporting Information. Adenosine 5′-triphosphate (ATP), adenosine 5′-diphosphate (ADP), and di-*tert*-butyl *N*,*N*-diethylphosphoramidite were obtained from Sigma (Germany). The P^3-1-(2-nitrophenyl)ethyl and P^3-1-(4,5-dimethoxy-2-nitrophenyl)ethyl esters of ATP (NPE- and DMNPE-caged ATP), fluo-3/AM, and Pluronic F-127 were acquired from Molecular Probes (USA). The remaining chemicals were of the highest grade commercially available and were used without further purification. Only HMPA was dried, over molecular sieves. TLC plates (silica gel, 60 F_{254}) were purchased from E. Merck (Germany). Acetonitrile and methanol were HPLC grade (Riedel – deHaën, Germany). Water was purified with a Milli-Q-Plus system (Millipore, Germany).

Instrumentation: Analytical HPLC was carried out on a Hewlett – Packard HP 1100 system (flow rate 1 mL min^{-1}) with diode array detector ($\lambda_{exc1} = 254$ nm, $\lambda_{exc2} = 385$ nm), fluorescence detector ($\lambda_{exc} = 385$ nm, $\lambda_{em} = 495$ nm), and a PLRP-S column (300 Å, 8 µm, 150 × 4.6 mm, from Polymer Laboratories Ltd. (UK)). Preparative

Figure 5. *Focal photorelease of ATP in acute brain slices. a) Fluorescence picture of the corpus callosum (cc) in acute mouse brain slices stained with fluo-3. Adjacent areas are indicated as cort. cer. (cortex cerebrum) and stria. (striatum). The release area is indicated as a square (34.2 × 34.2 µm, ROI 1). The sampling rate used for the recording was 2.5 Hz. The area shown is 921.3 × 921.3 µm. The white scale bar is 100 µm. b) Ca^{2+} ion transients in two individual cell bodies as marked by circles in (a). Traces represent the mean fluorescence in each ROI relative to the fluorescence before UV irradiation. ATP was released twice (dashed lines), which resulted in two Ca^{2+} ion transients. The rise in $[Ca^{2+}]_i$ is delayed according to the increasing distance from the release area. c) Analysis of the relationship between the propagating Ca^{2+} signal and diffusion of ATP in the slices. Data points show the onset time of the Ca^{2+} ion transient with respect to the distance from the illumination area for all responding cells. The curve shows the best fit of Equation (3) to the data points with the free parameters $c_{crit} = 4.9 \pm 0.9$ µM and $t_{delay} = 2.8 \pm 0.2$ s ($R^2 = 0.69$).*

HPLC was performed on a Shimadzu LC-8A system (flow rate: 10 mL min^{-1}) with a UV/Vis detector (SPD-6AV, $\lambda_{exc} = 254$ nm) on a Nucleogel RP 100 – 10 (300 × 25 mm) column from Macherey – Nagel (Germany). Mass spectra were determined by electrospray ionization mass spectrometry in the positive or negative ionization mode on a TSQ 700 (Finnigan MAT) spectrometer. ^{1}H and ^{31}P NMR spectra were measured on a Bruker DRX 600 NMR spectrometer. ^{1}H chemical shifts are given in parts per million (ppm) relative to tetramethylsilane as an internal standard. ^{31}P chemical shifts are reported in ppm referenced to external 85 % H_3PO_4. UV/Vis spectra were recorded on a UV/Vis spectrophotometer (Lambda 9, Perkin – Elmer). Fluorescence spectra were taken on a MPF-2A fluorescence spectrometer (Hitachi/Perkin – Elmer, Japan) combined with a personal computer plus a configured data analysis software package (SPECTRACALC). Photolysis of all employed caged compounds in solution was performed by use of a high-pressure mercury lamp (HBO 500, Oriel, USA) with controlled light intensity and corresponding metal interference transmission filters (334, 365, or 405 nm; Oriel, USA). The light intensity of the irradiation passing through each filter was registered by the power meter (model 1815-C plus detector 818-UV, Newport Corporation, USA) at the position of the cuvette. UV and fluorescence quartz cuvettes with a path length of 1 cm were used for all photochemical and photophysical experiments, respectively. During irradiation the solutions in the cuvettes were agitated with a small magnetic stirrer. All synthetic and analytical procedures were performed under yellow light provided by sodium vapor lamps.

Syntheses

***P*^{3}-[7-(Dimethylamino)coumarin-4-yl]methyl adenosine 5′-triphosphate trisodium salt (2), *P*^{2}-[7-(dimethylamino)coumarin-4-yl]methyl adenosine 5′-diphosphate disodium salt (3), and [7-(dimethylamino)coumarin-4-yl]methyl adenosine 5′-monophosphate sodium salt (4); Method A**: The disodium salt of ATP (551 mg, 1 mmol) was dissolved in water (20 mL) and adjusted to pH 4.2 with 1 N sodium hydroxide solution. Compound **1** (344 mg, 1.5 mmol) dissolved in chloroform (20 mL) was added, and the resultant mixture was vigorously stirred at room temperature in the dark for 24 h. The aqueous phase was separated, washed three times with chloroform (each 10 mL), and evaporated in vacuo. The reaction products **2** – **4** were separated by preparative HPLC by use of a linear gradient procedure for elution as follows: 0 – 10 min, 0 % B in A; 10 – 60 min, 0 – 30 % B in A; 60 – 85 min, 30 – 100 % B in A; eluent A was triethylammonium acetate (5 mM) in water (pH 7.0), and eluent B was methanol. The triethylammonium salts of **2** (r.t.: 56.3 min, 20.1 mg; r.t. = retention time), **3** (r.t.: 66.0 min, 37.2 mg), and **4** (r.t.: 79.6 min, 16.6 mg) obtained after lyophilization were hygroscopic substances. They were therefore converted into their corresponding sodium salts by loading onto a cation exchanger column (filled with Dowex 50 WX-2 and charged with sodium ions), elution with water, evaporation, and purification by preparative HPLC (same conditions as above, but eluent A was water instead of 5 mM triethylammonium acetate buffer). Yields: 14.1 mg of **2** (1.7 %), 26.1 mg of **3** (3.5 %), and 11.6 mg of **4** (1.7 %).

Compounds 2 and 3, Method B: Compounds **2** and **3** were synthesized by the procedure described for *P*^{2}-[7-(diethylamino)coumarin-4-yl]methyl cytidine 5′-diphosphate,[17] from ADP (free acid, 76.9 mg, 180 μmol) and AMP (free acid, 65.7 mg, 180 μmol), respectively, tri-*n*-octylamine (87.9 μL, 360 μmol for ADP and 44.0 μL, 180 μmol for AMP), carbonyldiimidazole (117 mg, 720 μmol), **7** (36 mg, 120 μmol), and tri-*n*-butylamine (28.6 μL, 120 μmol) by stirring in HMPA (2 mL, for ADP) or in DMF (2 mL, for AMP) at room temperature for 3 days. The solvents were removed in vacuo and the raw materials were purified by preparative HPLC (same conditions as in Method A). The triethylammonium salts of **2** (r.t.: 56.3 min) and **3** (r.t.: 66.0 min) formed were converted into their corresponding sodium salts and purified as described in Method A to give 21 mg (20 %) of **2** (12 mg ≈ 13 % of **3** as by-product) and 21 mg (23 %) of **3**.

Data for compound 2: ^{1}H NMR (600 MHz, D_2O): $\delta = 2.87$ (s, 6H), 4.17 – 4.19 (m, 2H), 4.23 – 4.31 (m, 3H), 4.94 – 5,03 (m, 2H), 5.69 (d, J = 4.0 Hz, 1H), 6.12 (m, 2H), 6.34 (dd, J = 9.1, 2.5 Hz, 1H), 7.01 (d, J = 9.0 Hz, 1H), 7.95 (s, 1H), 8.11 (s, 1H) ppm; ^{31}P NMR (243 MHz, D_2O) heteronuclear decoupled: $\delta = -10.8$, -11.1 (α and γ P_i), -22.5 (β P_i) ppm; MS: *m/z*: 707.35 (free acid) $[M-H]^-$; elemental analysis: calcd (%) for $C_{22}H_{24}N_6O_{15}P_3Na_3 \cdot 4.5\,H_2O$ (855.43): C 30.89, H 3.89, N 9.82; found: C 30.83, H 3.93, N 9.94.

Data for compound 3: ^{1}H NMR (600 MHz, D_2O): $\delta = 2.83$ (s, 6H), 4.13 – 4.15 (m, 1H), 4.26 – 4.27 (m, 2H), 4.33 – 4.36 (m, 2H), 4.90 (m, 2H), 5.73 (d, J = 4.5, 1H), 5.97 (d, J = 2.2 Hz, 1H), 6.05 (s, 1H), 6.26 (dd, J = 8.7, 2.5 Hz, 1H), 6.84 (d, J = 8.8 Hz, 1H), 7.88 (s, 1H), 8.05 (s, 1H) ppm; ^{31}P NMR (243 MHz, D_2O) heteronuclear decoupled: $\delta = -11.1$ (α and β P_i) ppm; MS: *m/z*: 627.22 (free acid) $[M-H]^-$; elemental analysis: calcd (%) for $C_{22}H_{24}N_6O_{12}P_2Na_2 \cdot 4.5\,H_2O$ (753.46): C 35.09, H 4.19, N 11.05; found: C 35.18, H 4.24, N 11.00.

Data for compound 4: ^{1}H NMR (600 MHz, D_2O): $\delta = 2.92$ (s, 6H), 4.14 – 4.16 (m, 1H), 4.27 – 4.28 (m, 1H), 4.32 (s, 1H), 4.39 – 4.40 (m, 1H), 4.49 – 4.50 (m, 1H), 4.69 (d, J = 15.5 Hz, 1H), 4.92 (d, J = 15.5 Hz, 1H), 5.84 (d, J = 4.5 Hz, 1H), 6.01 (d, J = 2.2 Hz, 1H), 6.10 (s, 1H), 6.24 (dd, J = 7.4, 2.5 Hz, 1H), 6.71 (d, J = 7.4 Hz, 1H), 7.95 (s, 1H), 8.04 (s, 1H) ppm; ^{31}P NMR (243 MHz, D_2O) heteronuclear decoupled: δ = 0.95 ppm; MS: *m/z*: 547.22 (free acid) $[M-H]^-$; elemental analysis: calcd (%) for $C_{22}H_{24}N_6O_9P_1Na_1 \cdot 5.5\,H_2O$ (669.51): C 39.47, H 5.27, N 12.55; found: C 39.34, H 4.83, N 11.78.

UV/Vis spectroscopy, photochemical quantum yield, and comparison of photoefficiencies: Solutions of **2** – **4** (25 μM) in HEPES buffer (20 mM HEPES and 240 mM KCl adjusted to pH 7.2 with 1 N KOH) were used for UV/Vis spectroscopy.

The differential photochemical quantum yield Φ_{chem}, defined as the ratio of the number of molecules converted to the number of absorbed photons, was determined for **2** – **4** by a relative method[24] on the basis of the equation $\Phi_{chem} = (dc/dt) \times (I_{abs})^{-1} \times V$, with the axial isomer of [7-(diethylamino)coumarin-4-yl]methyl-caged 8-bromoguanosine 3′,5′-cyclic monophosphate (*ax*-DEACM-caged 8-Br-cGMP; $\Phi_{chem} = 0.27$[16]) as a standard (for details see the Supporting Information).

To compare the photoefficiency of **2** with those of commercially available ATP-phototriggers, 25-μM solutions of **2** and DMNPE- and NPE-caged ATP were irradiated at 334, 365, and 405 nm, with stirring. The photodecomposition of the caged ATPs was analyzed by HPLC as described for **2** – **4** in the Supporting Information.

Fluorescence spectroscopy, fluorescence quantum yield, and time-resolved fluorescence spectroscopy: To minimize photolysis of **2** – **4** during the investigations, this analysis was performed with very low excitation intensities and very short registration times.

The fluorescence spectra of **2** – **4** (25 μM) were measured in HEPES buffer. The fluorescence quantum yields (Φ_f) of **2** – **4** were determined at 298 K by the relative method[25] versus quinine sulfate in 0.1 N H_2SO_4 as a standard ($\Phi_{f,s} = 0.546$[26]). The optical densities of the solutions of **2** – **4** in HEPES buffer and that of the standard were adjusted to identical values (0.3 – 0.5) in the range of the excitation wavelength (from 357 to 358 nm). The different refractive indices of the solutions were taken into account in the calculation.

Time-resolved fluorescence rise and decay curves were recorded in right-angle arrangement.[27, 20] As excitation source we used an MSC 1600 N_2 laser from LTB ($\lambda_{exc} = 337$ nm, pulse width 0.5 ns, maximum pulse energy 0.7 mJ). Excitation was carried out in 1 cm ×

1 cm fluorescence quartz cells, observed through appropriate interference filters ($\lambda_{em} = 500$ nm) with a wide aperture collection lens and detected by an amplified AD 110 silicon avalanche diode from opto-electronics, with a rise time of 600 ps. All signals were digitized and fed into a Tektronix TDS 620A storage oscilloscope. The apparatus function was obtained by irradiation of a layer of MgO with N_2 laser pulses and recording the light reflected by the setup. Here the signal was averaged over 50 laser shots. In the case of **5**, signals were also averaged to improve the signal-to-noise ratio further, whereas with photolabile caged compounds only single-shot experiments were allowed.

The evaluation of the decay time of **5** was performed by nonlinear least-squares fitting routines and convoluting the apparatus function with the monoexponential decay function. For the signals of the caged compounds, convolution was performed with a biexponential rise and decay function with the known lifetime of **5** as the one fixed decay constant. The achieved time resolution was about 200 ps.

Preparation of cell cultures: Astrocytes were prepared from cortex tissue of newborn NMRI mice as described previously.[28] Briefly, cortical tissue was carefully freed from blood vessels and meninges, trypsinized, and gently triturated with a fire-polished pipette in the presence of 0.05% DNAase (Worthington Biochem. Corp., Freehold, USA). The tissue was then washed twice with Hank's Balanced Salt Solution (HBSS), resuspended in Eagle's Basal Medium (BME; Seromed, Berlin, Germany) containing 10% heat-inactivated fetal calf serum (FCS; Gibco), penicillin (100 I.U. mL^{-1}), and streptomycin (100 μg mL^{-1}) (BME/FCS). DNase was added to produce a final concentration of 0.05% and the tissue was triturated through Pasteur pipettes to yield a single-cell suspension. The suspension was centrifuged at 800 rpm for 10 min at 4 °C and washed twice with ice-cold HBSS. After resuspension in BME/FCS medium, cells were plated on poly-L-lysine-coated (100 μg mL^{-1}; Sigma, Deisenhofen, Germany) coverslips (with approximately the cells from one brain per petri dish), and then incubated at 37 °C in 5% CO_2 atmosphere. One day later, cultures were washed twice with HBSS to remove cellular debris and maintained in BME/FCS medium for 4 days. After a subconfluent state was reached, cellular debris, microglia cells, oligodendrocytes, and their early precursor cells were dislodged by manual shaking and removed by washing the cultures three times with HBSS.

The purity of the prepared astrocyte cultures was routinely determined by immunofluorescence with a polyclonal antibody against glial fibrillary acidic protein (GFAP; DAKO, Hamburg, Germany), and dichlorotriazinylamino fluorescent-conjugated or Cy3-conjugated secondary antibodies (Boehringer, Mannheim, Germany). Subconfluent monolayer prepared of cells showed more than 90% positive staining for GFAP, a specific astrocyte marker.

Preparation of acute brain slices: For acute brain slice preparations, mice were decapitated and the brain was immediately removed. The forebrain was glued to a glass block and frontal sections of 250 μm were cut with a vibratome (Leica Microsystems AG, Wetzlar, Germany). Slicing was performed in ice-cold bicarbonate-buffered salt solution gassed with carbogene (5% CO_2 and 95% O_2). This bath solution contained (mM): NaCl (134), KCl (2.5), $MgCl_2$ (1.3), $CaCl_2$ (2), K_2HPO_4 (1.25), $NaHCO_3$ (26), and D-glucose (10). The brain slices were kept in bath solution at room temperature until used for measurements.

Optical Ca^{2+} measurements by confocal laser scanning microscope (CLSM): These studies were performed on an LSM 510 inverted confocal laser scanning microscope (Carl Zeiss Jena GmbH, Germany) with a 10 ×/0.5 objective. The cell cultures and the brain slices, respectively, were loaded with the Ca^{2+} indicator fluo-3/AM (4.4×10^{-6} M in the buffer medium in the presence of 0.01% Pluronic F-127) for 30 min at 37 °C in darkness, then washed three times and incubated for another 30 min in the buffer medium to allow complete hydrolysis of the AM ester. The fluo-3 experiments were conducted with an argon laser ($\lambda = 488$ nm) for excitation. The excitation wavelength was directed onto the sample by means of a dichroic mirror (FT 490). The fluorescence intensities were detected at wavelengths greater than 505 nm by using an additional cut-off filter (LP 505) in front of the detector. Fluorescence images were usually scanned and stored as time series.

Photorelease of 2 in the CLSM: Coverslips with cultured astrocytes were mounted on a perfusion chamber and perfused with HEPES buffer until the start of recording. Perfusion was then stopped, and a stock solution of **2** in HEPES buffer (100 μL) was added to produce a final concentration of **2** of 500 μM. Similarly, brain slices were placed in a chamber ($V \approx 500$ μL) and perfused with bicarbonated artificial cerebral brain fluid until the beginning of the experiment. Here, buffer was superficially gassed to maintain pH buffering and a stock solution of **2** (100 μL) was added. To attain an equal concentration distribution, the final solution was incubated for 5 min (final concentration of **2**: 1 mM). Compound **2** was photolyzed by use of a continuous wave argon ion laser ($\lambda = 364$ nm, Coherent, Germany). This UV laser is integral to the confocal system (part of the commercially available LSM 510 inverted setup) and tracks, in the normal scanning mode of the instrument, point-by-point in a line (X-direction) and also line-by-line (Y-direction) over the image. The cross-sectional area of the UV laser could be confined to a small region of interest within the imaging area.

General setup for Ca^{2+} measurements with 2 in the CLSM: For rapid Ca^{2+} measurements we typically scanned an area of 921.3 × 921.3 μm with 512 × 512 pixel resolution at time intervals of 400 ms. Before each measurement we defined an ROI for the UV irradiation (e.g., 10.8 × 10.8 μm). After the start of the time series, UV irradiation could be manually triggered for a predefined duration. For analysis, images of the time series were computed offline by use of the Laser Scanning Microscope LSM 510/Version 3.0 SP 2 (Carl Zeiss GmbH, Germany) confocal system software.

Recorded fluorescence images before UV irradiation (about 30) were used to define a control (F_0) for each evaluated cell. Changes in Ca^{2+} concentration within the cells were monitored by changes in the fluorescence intensity (F) relative to F_0 and displayed as relative fluorescence intensity (F/F_0).

Nonlinear diffusion fitting procedure: To test for correlation between ATP diffusion and the resulting fluorescent Ca^{2+} signal, we used the following model to describe the ATP diffusion. The concentration of liberated ATP is considered to be uniform in the release volume regarding the transverse direction, since only a relatively small fraction of the incident light is actually absorbed. This assumption is based on the measured UV laser intensity of 0.7 mW (Newport power meter, for details see the Instrumentation section) at the coverslip position (that is, the calculated number of absorbed photons per second exceeds the number of molecules of **2** in the irradiation volume by approximately two orders of magnitude). Diffusion will then lie in the two-dimensional plane of the buffer solution. Since the release area is small compared to the extension of the propagating Ca^{2+} signal, we approximated the initial ATP concentration to be concentrated axial to the release area [Eq. (1)].

$$c(\vec{r}, t = 0) = \delta(x) \cdot \delta(y) \cdot \rho(z) \quad (1)$$

In this equation, c is the concentration of ATP, t is time since ATP release, and $\vec{r}$ is the distance from the release point. The solution of

the general diffusion equation for this initial concentration distribution is than given by Equation (2),

$$c(\vec{r},t) = \frac{\rho}{4\pi Dt}\cdot\exp\left(-\frac{r^2}{4Dt}\right) \quad (2)^{[29]}$$

that is, the concentration distribution shows a Gaussian profile collapsing with t (D is the diffusion coefficient of ATP = 368 $\mu m^2 s^{-1}$).[30]

The time-dependent spatial expansion of the particles described by the time-dependent distance of a threshold concentration c_t from the initial release point is therefore given by Equation (3).

$$r(t) = 2\sqrt{Dt\cdot\ln\left(\frac{\rho}{c_t\cdot 4\pi\cdot Dt}\right)} \quad (3)$$

The logarithm turns negative with t and therefore the square root turns imaginary, which describes the finite maximum expansion of a selected c_t value.

We compared the temporal development of the propagating Ca^{2+} ion wave by Marquardt – Levenberg nonlinear regression of Equation (3) by use of the Origin 6.1 program (Microcal, USA). The c_t value was kept as a free parameter and t was substituted with $t' = t_0 - t_{delay}$ to allow for delay between ATP diffusion and corresponding Ca^{2+} response.

We thank B. Dekowski, B. Gentsch, J. Loßmann, and B. Gerlach for technical assistance. We are grateful to Dr. R. Schmidt and C. Schweitzer (Institut für physikalische und theoretische Chemie, Johann-Wolfgang-Goethe Universität Frankfurt/Main, Germany) for the time-resolved fluorescence measurements, and to S. Serowy (FMP) for helpful discussions. This work was supported by the Deutsche Forschungsgemeinschaft and the Fonds der Chemischen Industrie.

[1] a) Y. Kao, S. R. Adams, *Optical Microscopy: Emerging Methods and Applications*, Academic Press, San Diego, **1993**, pp. 27 – 85; b) S. R. Adams, R. Y. Tsien, *Annu. Rev. Physiol.* **1993**, *55*, 755 – 784; c) J. E. T. Corrie, D. R. Trentham, *Bioorganic Photochemistry, Volume 2: Biological Applications of Photochemical Switches*, Wiley, Chichester, **1993**, pp. 243 – 305; d) *Methods Enzymol.* (Ed.: G. Marriott), **1998**, *291*.

[2] J. H. Kaplan, B. F. Forbush III, J. F. Hoffmann, *Biochemistry* **1978**, *17*, 1929 – 1935.

[3] J. W. Walker, G. P. Reid, J. A. McCray, D. R. Trentham, *J. Am. Chem. Soc.* **1988**, *110*, 7170 – 7177.

[4] J. E. T. Corrie, G. P. Reid, D. R. Trentham, M. B. Hursthouse, M. A. Mazid, *J. Chem. Soc. Perkin Trans. 1* **1992**, 1015 – 1019.

[5] J. W. Wootton, D. R. Trentham, *NATO ASI Ser., Ser. C*, **1989**, *272*, 277 – 296.

[6] C.-H. Park, R. S. Givens, *J. Am. Chem. Soc.* **1997**, *119*, 2453 – 2463.

[7] H. Thirlwell, J. E. T. Corrie, G. P. Reid, D. R. Trentham, M. A. Ferenczy, *Biophys. J.* **1994**, *67*, 2436 – 2447.

[8] R. S. Givens, C.-H. Park, *Tetrahedron Lett.* **1996**, *35*, 6259 – 6262.

[9] V. S. Sokolov, H. J. Apell, J. E. T. Corrie, D. R. Trentham, *Biophys. J.* **1998**, *74*, 2285 – 2298.

[10] S. Geibel, A. Barth, S. Amslinger, A. H. Jung, C. Burzik, R. J. Clarke, R. S. Givens, K. Fendler, *Biophys. J.* **2000**, *79*, 1346 – 1357.

[11] V. Hagen, J. Bendig, S. Frings, T. Eckardt, S. Helm, D. Reuter, U. B. Kaupp, *Angew. Chem.* **2001**, *113*, 1078 – 1080; *Angew. Chem. Int. Ed.* **2001**, *40*, 1046 – 1048.

[12] T. Eckardt, V. Hagen, B. Schade, R. Schmidt, C. Schweitzer, J. Bendig, *J. Org. Chem.* **2002**, *67*, 703 – 710.

[13] P. B. Guthrie, J. Knappenberger, M. Segal, M. V. Bennett, A. C. Charles, S. B. Kater, *J. Neurosci.* **1999**, *19*, 520 – 528.

[14] a) C. H. Kastritsis, A. K. Salm, K. McCarthy, *J. Neurochem.* **1992**, *58*, 1277 – 1284; b) B. Pearce, D. Langley, *Brain Res.* **1994**, *660*, 329 – 332.

[15] B. Pearce, S. Murphy, J. Jeremy, C. Morrow, P. Dandona, *J. Neurochem.* **1989**, *52*, 971 – 977.

[16] a) V. Hagen, S. Frings, B. Wiesner, S. Helm, U. B. Kaupp, J. Bendig, unpublished results; b) The photochemical quantum yield of ax-DEACM-caged 8-Br-cGMP was determined by potassium ferrioxalate actinometry.

[17] O. Schönleber, J. Bendig, V. Hagen, B. Giese, *Bioorg. Med. Chem.* **2002**, *10*, 97 – 101.

[18] K. Ito, K. Maruyama, *Chem. Pharm. Bull.* **1983**, *31*, 3014 – 3023.

[19] B. Schade, V. Hagen, R. Schmidt, R. Herbrich, E. Krause, T. Eckardt, J. Bendig, *J. Org. Chem.* **1999**, *64*, 9109 – 9117.

[20] R. Herbrich, R. Schmidt, *J. Photochem. Photobiol. A* **2000**, *133*, 149 – 158.

[21] A. Barth, K. Hauser, W. Mäntele, J. E. T. Corrie, D. R. Trentham, *J. Am. Chem. Soc.* **1995**, *117*, 10311 – 10316.

[22] J. D. Troadec, S. Thirion, D. Petturiti, M. T. Bohn, P. Poujeol, *Pfluegers Arch.* **1999**, *437*(5), 745 – 753.

[23] C. G. Schipke, C. Boucsein, C. Ohlemeyer, F. Kirchhoff, H. Kettenmann, *FASEB J.* **2002**, *16*(2), 255 – 257.

[24] V. Hagen, C. Dzeja, S. Frings, J. Bendig, E. Krause, U. B. Kaupp, *Biochemistry* **1996**, *35*, 7762 – 7771.

[25] J. N. Demas, G. A. Crosby, *J. Phys. Chem.* **1971**, *75*, 991 – 999.

[26] H. G. O. Becker, H. Böttcher, F. Dietz, D. Rehorek, G. Roewer, K. Schiller, H.-J. Timpe, *Einführung in die Photochemie*, Deutscher Verlag der Wissenschaften, Berlin, **1991**, p. 455.

[27] C. Grewer, H.-C. Brauer, *J. Phys. Chem.* **1993**, *97*, 5001 – 5006.

[28] S. Lyons, H. Kettenmann, *J. Cereb. Blood Flow Metab.* **1998**, *18*(5), 521 – 530.

[29] L. D. Landau, E. M. Lifschitz, *Lehrbuch der theoretischen Physik*, *Band VI*, Akademie Verlag, Berlin, **1966**, p. 262.

[30] M. J. Hubley, B. R. Locke, T. S. Moerland, *Biochim. Biophys. Acta.* **1996**, *1291*(2), 115 – 121.

Received: July 26, 2002 [F461]